

# Competitions of Superconducting, Antiferromagnetic and Charge Orders with Intervention by Phase Separation in 2D Holstein-Hubbard Model

Takahiro Ohgoe and Masatoshi Imada  
 Department of Applied Physics, University of Tokyo,  
 7-3-1 Hongo, Bunkyo-ku, Tokyo 113-0033, Japan  
 (Dated: March 28, 2017)

Using a variational Monte Carlo method, we study competitions of strong electron-electron and electron-phonon interactions in the ground state of Holstein-Hubbard model on a square lattice. At half filling, an extended intermediate metallic or weakly superconducting (SC) phase emerges, sandwiched by antiferromagnetic (AF) and charge order (CO) insulating phases. By the carrier doping into the CO insulator, the SC order dramatically increases for strong electron-phonon couplings, but largely hampered by wide phase separation (PS) regions. Superconductivity is optimized at the border to the PS.

PACS numbers: 63.20.Kr, 71.10.Fd, 71.27.+a, 74.25.Kc, 74.72.-h

*Introduction.* —The electron-phonon interaction in condensed matter is the origin of many important phenomena such as conventional superconductivity (SC) and charge density wave. In a class of strongly-correlated materials, the interplay between electron correlations and electron-phonon interactions is believed to induce novel phenomena such as the unconventional high- $T_c$   $s$ -wave SC in the alkali-doped fullerenes[1–3]. Even for high- $T_c$  cuprates, some experiments[4] and theoretical studies[5–7] have suggested the important roles of phonons for full understanding the electronic properties including the SC. However, they are still controversial because the relevance of the electron-phonon interaction addressed in previous theoretical works largely rely on adjustable model parameters introduced in an *ad hoc* fashion. In addition, computationally accurate framework to study the interplay between the electron correlation and the electron-phonon interaction has not fully been explored. To establish the roles of phonons in a wide range of strongly correlated materials including the cuprates, we need a flexible method which can accurately treat strong electron-electron and electron-phonon interactions on an equal footing.

For decades, variational Monte Carlo (VMC) methods have been applied to investigate strongly correlated electrons[8–10]. Its advantage is that it does not suffer from the notorious negative-sign problem, whereas its accuracy depends on the assumed variational wave function. However, owing to the improved efficient optimization method such as the stochastic reconfiguration method[11], its accuracy and flexibility have improved by introducing many variational parameters[12–19]. It has been recently applied to complicated *ab-initio* multi-orbital effective Hamiltonians[20–22]. Recently, we have successfully extended this many-variable VMC (mVMC) method to electron-phonon coupled systems[23].

The Holstein-Hubbard model is the simplest model for studying the interplay of electron-electron and electron-phonon interactions. However, the phase diagram and physical properties under these two competing interactions are far from complete understanding even for the

ground states. In one dimension and the Bethe lattice with infinite coordination, its phase diagrams have been obtained by the density matrix renormalization group (DMRG)[24–26] and the dynamical mean-field theory (DMFT)[27, 28], respectively. At half filling, the DMRG studies have established the presence of an intermediate metallic phase between a Mott insulating and a CO phases in the ground-state phase diagram. On the other hand, the DMFT study for zero temperature has not found its evidence[27]. For square lattices, a finite-temperature quantum Monte Carlo (QMC) study has also suggested the emergence of an intermediate paramagnetic metallic phase between the AF and CO phases[29, 30]. However, such a phase diagram cannot be conclusive in the finite-temperature studies because of the Mermin-Wagner theorem.

Another important open issue is found when carriers are doped into the half-filled system. The DMFT study on the Holstein model has revealed the presence of a coexisting phase of CO and SC which is not prevented by the PS[31]. It is interesting to ask whether the coexistence also exists in two dimensions. The connection between the SC and PS is also intriguing and has been discussed in the literature[32, 33] for a different context of the three-band Hubbard model as a model for the cuprates. Recently, their strong connections are observed in the mVMC studies on the Hubbard model[15] and *ab-initio* effective Hamiltonian of electron-doped LaFeAsO[21]. A natural question here is whether a phonon-driven PS also has a connection in the case of the  $s$ -wave SC. In this paper, we study these issues by using the many-variable VMC method.

*Model.* —The Hamiltonian we consider here is given by

$$\mathcal{H} = -t \sum_{\langle i,j \rangle, \sigma} (c_{i\sigma}^\dagger c_{j\sigma} + \text{h.c.}) + U \sum_i n_{i\uparrow} n_{i\downarrow} + g \sum_i x_i n_i + \sum_i \left( \frac{p_i^2}{2M} + \frac{M\Omega^2 x_i^2}{2} \right), \quad (1)$$

where  $t$ ,  $U$ ,  $g$ , and  $\Omega$  represent the hopping amplitude,

the on-site interaction strength between electrons, the electron-phonon interaction strength, and the phonon frequency, respectively.  $c_{i\sigma}(c_{i\sigma}^\dagger)$  represents the annihilation (creation) operator of an electron with spin  $\sigma$  ( $=\uparrow$  or  $\downarrow$ ) at the site  $i$ . The particle number operators  $n_{i\sigma}$  and  $n_i$  are defined by  $n_{i\sigma} = c_{i\sigma}^\dagger c_{i\sigma}$  and  $n_i = n_{i\uparrow} + n_{i\downarrow}$ .  $x_i$  and  $p_i$  are the lattice displacement operator and its conjugate momentum operator, respectively.  $x_i$  relates to the annihilation/creation boson(phonon) operator  $b_i/b_i^\dagger$  as  $x_i = \sqrt{\frac{1}{2M\Omega}}(b_i + b_i^\dagger)$ . The dimensionless electron-phonon interaction strength  $\lambda$  is defined as the ratio of the lattice deformation energy to half the bandwidth  $W/2 = 4t$  and we obtain  $\lambda = g^2/(M\Omega^2W)$ , where  $M$  is the mass of single-component nuclei. If we consider the path-integral representation of the partition function and integrate out the phonon degrees of freedom, the model is exactly mapped onto the Hubbard model with the effective dynamical on-site interaction  $U_{\text{eff}}(\omega) = U - \frac{\lambda W}{1 - (\omega/\Omega)^2}$ . In this paper, we set  $M = t = 1$  as the unit of mass and energy. We consider  $N = L^2$  systems on the square lattice with  $N_e$  electrons and impose the periodic/anti-periodic boundary condition in the  $x/y$ -direction to satisfy the closed-shell condition. The filling factor and doping (hole) concentration are given by  $\rho = N_e/N$  and  $\delta = 1 - \rho$ , respectively.

*Method.* — Our variational wave function for electron-phonon coupled systems takes the following form:  $|\psi\rangle = \mathcal{P}^{\text{el-ph}}(|\psi^{\text{el}}\rangle|\psi^{\text{ph}}\rangle)$ [23]. Here,  $|\psi^{\text{el}}\rangle$  and  $|\psi^{\text{ph}}\rangle$  represent variational wave functions for electrons and phonons, respectively.  $\mathcal{P}^{\text{e-ph}}$  is the electron-phonon correlation factor which takes into account the entanglement between electrons and phonons. Its explicit form is given by  $\mathcal{P}^{\text{el-ph}} = \exp\left(\sum_{i,j} \alpha_{ij} x_i n_j\right)$ , where  $\alpha_{ij}$  are variational parameters. As an electron variational wave function, we adopt the generalized pairing wave function with the Gutzwiller[34] and Jastrow correlation factors[35]:  $|\psi^{\text{el}}\rangle = \mathcal{P}^{\text{J}}\mathcal{P}^{\text{G}}|\phi^{\text{pair}}\rangle$ . The generalized pairing wave function takes the form of  $|\phi^{\text{pair}}\rangle = \left(\sum_{i,j=1}^N f_{ij} c_{i\uparrow}^\dagger c_{j\downarrow}^\dagger\right)^{N_e/2} |0\rangle$ , where  $f_{ij}$  are variational parameters. This is a generalization of the Hartree-Fock-Bogoliubov type wave function with AF/CO and SC orders[13, 36] and thus flexibly describes these states as well as paramagnetic metals (PM). For  $f_{ij}$ , we assume a  $2\times 2$  sublattice structure and thus the number of its variational parameters is  $2\times 2\times N$ . For a phonon wave function, we use the tensor product of phonon wave functions with wave vectors  $\mathbf{q}$ :  $|\psi^{\text{ph}}\rangle = \prod_{\mathbf{q}} |\psi_{\mathbf{q}}^{\text{ph}}\rangle$ .  $|\psi_{\mathbf{q}}^{\text{ph}}\rangle$  is expanded in terms of phonon Fock states  $|m_{\mathbf{q}}\rangle$  as  $|\psi_{\mathbf{q}}^{\text{ph}}\rangle = \sum_{m_{\mathbf{q}}=0}^{m_{\mathbf{q}}^{\text{max}}} c_{m_{\mathbf{q}}} |m_{\mathbf{q}}\rangle$ . Here,  $m_{\mathbf{q}}^{\text{max}}$  are controllable cutoffs for the number of phonons and  $c_{m_{\mathbf{q}}}$  are treated as variational parameters of real numbers. The number of its variational parameters is  $\sum_{\mathbf{q}} (m_{\mathbf{q}}^{\text{max}} + 1)$ , which is equal to  $N(m^{\text{max}} + 1)$  if we take  $m_{\mathbf{q}}^{\text{max}} = m^{\text{max}}$ . In this study, we checked the convergence of physical quantities as a function of the cutoff and we typically took

$m_{\mathbf{q}}^{\text{max}} = 10 - 40$  for  $\mathbf{q} = (\pi, \pi)$  and  $m_{\mathbf{q}}^{\text{max}} = 5$  for others. As initial states in the optimization of variational parameters, we considered the non-interacting Fermi sea (PM state), SC, AF, CO, and coexisting states of SC+AF and SC+CO.

*Half-filled case.* — We consider two phonon frequencies: An intermediate frequency  $\Omega = 8t$  (equal to the bandwidth  $W$ ) and a smaller one  $\Omega = t$ . In Fig. 1, we summarize our results in the ground-state phase diagram in the  $U - \lambda$  plane. The phase diagram includes the boundary of the AF and CO phases. To distinguish each phase, we measured the spin structure factor  $S_s(\mathbf{q}) = \frac{1}{3N} \sum_{i,j} \langle \mathbf{S}_i \cdot \mathbf{S}_j \rangle e^{i\mathbf{q} \cdot (\mathbf{r}_i - \mathbf{r}_j)}$  and the charge structure factor  $S_c(\mathbf{q}) = \frac{1}{N} \sum_{i,j} (\langle n_i n_j \rangle - \rho^2) e^{i\mathbf{q} \cdot (\mathbf{r}_i - \mathbf{r}_j)}$ . For  $\Omega = 8t$ , we found a wide intermediate region between the AF phase and CO phases. For smaller frequency  $\Omega = t$ , previous quantum Monte Carlo studies suggested the presence of an intermediate PM region at  $U = 5t$  and at finite temperature  $T/t = 0.25$ [29, 30]. However, *at zero temperature*, we found the intermediate region only for  $U \lesssim 2$ . The shrinkage of the intermediate region for small  $\Omega$  is also observed in one[24, 25] and infinite[28] dimensions.

In Fig. 2 (a) and (b), we plot the spin/charge structure factor  $S_{s/c}(\pi, \pi)/N$  as a function of  $\lambda$  at  $(U/t, \Omega/t) = (8, 8)$  and  $(U/t, \Omega/t) = (8, 1)$ , respectively. In the antiadiabatic limit  $\Omega \rightarrow \infty$ , the model is mapped to the standard Hubbard model with the on-site interaction  $U_{\text{eff}} = U - W\lambda$  where the order parameter  $m_{s/c} = \sqrt{\lim_{L \rightarrow \infty} S_{s/c}(\pi, \pi)/N}$  has an essential singularity at  $U_{\text{eff}} = 0$  (which corresponds to  $\lambda = 1$  for  $U = 8t$ )[37]. Here, we assume the Hartree-Fock predictions of  $|U_{\text{eff}}| m_{s/c} \sim t e^{-2\pi\sqrt{|t/U_{\text{eff}}|}}$  (as suggested in Fig. 25 of [38]) and we plot  $|U_{\text{eff}}|/t |m_{s/c}|$  as a function of  $\sqrt{|t/U_{\text{eff}}|}$  in the inset of Fig. 2 (a). However, the data do not follow this essential singular behavior in the intermediate region. Instead,  $m_{s/c}$  vanishes at a first-order transition before reaching the asymptotic weak-coupling region. Furthermore, we observe energy crossings which are also indications of first-order transitions (see Supplementary Materials). The limit of  $\Omega/t \rightarrow 0$  with the spring constant  $K = M\Omega^2$  kept fixed ( $M \rightarrow \infty$ ) is called adiabatic (classical) limit. In this limit, the ground state at  $\lambda = 0$  should be preserved for nonzero  $\lambda$  unless the static lattice deformation occurs. Even for  $\Omega = t$ , we found that physical quantities such as  $S_s(\pi)/N$  is still insensitive to  $\lambda$  until the first-order transition to the CO phase. In the intermediate region, it is likely that weak SC orders emerge, while expected amplitudes of the order are too weak so that we could not distinguish them from PM states in the available data of finite systems (see Supplementary Materials).

*Doped case.* — We study the doped region in the Holstein model ( $U = 0$ ). Although we here consider the case of  $U = 0$  where  $U_{\text{eff}} = -W\lambda (< 0)$ , given the adiabatic continuity suggested in Fig. 1, we expect essentially similar behaviors for  $U > 0$  if we consider the same value of

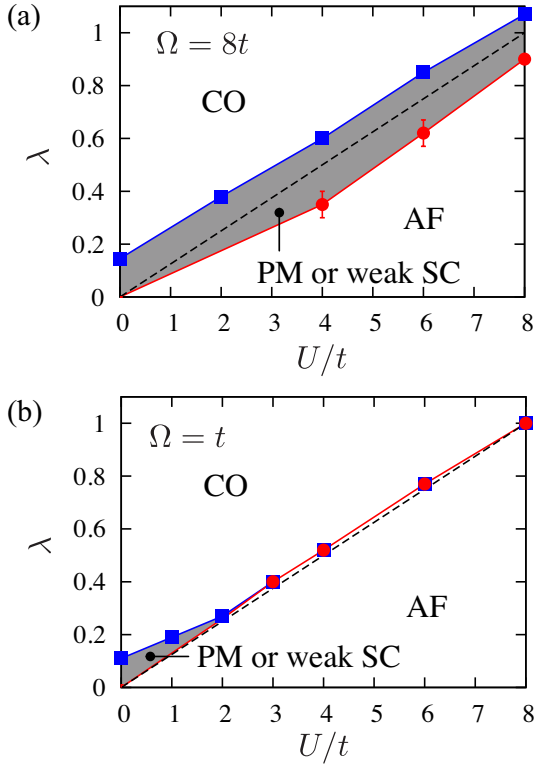


FIG. 1: (Color online) Ground-state phase diagram of the half-filled Holstein-Hubbard model on a square lattice at (a)  $\Omega = 8t$  and (b)  $\Omega = t$ . The blue squares and red circles represent the boundaries of CO and AF, respectively. Error bars are drawn, but most of them are smaller than the symbol size. Lines are used to guide the eye. Based on the fact that if  $\lambda = 0$ , the system is an AF insulator for any  $U > 0$ [37], we put the starting point of the AF boundary at the origin. Shaded region represents the intermediate PM or weak SC region.

$U_{\text{eff}} = U - W\lambda (< 0)$ . In Fig. 3, we present our ground-state phase diagram in the  $\delta - \lambda$  plane for  $\Omega = 8t$  and  $\Omega = t$ . For  $U = 0$ , the effective interaction  $U_{\text{eff}}(\omega)$  has negative parts for  $\omega < \Omega$ , which lead to  $s$ -wave SC states except for the gapped CO phase at half filling. In our phase diagram, the SC + CO phase is absent. Instead, the PS region appears adjacent to the CO phase at half filling. We find that for the smaller phonon frequency, the PS region is enlarged. In the supplemental material, we present the phase diagram in the adiabatic limit as the extreme case. In Fig. 3, we also plot  $S_c(\pi, \pi)/N$  and the long-range part of the  $s$ -wave SC correlation function  $P_s^\infty$  which is defined by  $P_s^\infty = \frac{1}{M} \sum_{\sqrt{2}L/4 < |\mathbf{r}|} P_s(\mathbf{r})$ . Here,  $\mathbf{r}$  is the relative position vectors belonging to  $(-L/2, L/2]^2$  and  $M$  is the number of vectors satisfying  $\sqrt{2}L/4 < |\mathbf{r}| < \sqrt{2}L/2$  and the SC function  $P_s(\mathbf{r})$  is defined by  $P_s(\mathbf{r}) = \frac{1}{N} \sum_{\mathbf{r}_i} \langle \Delta_s^\dagger(\mathbf{r}_i) \Delta_s(\mathbf{r}_i + \mathbf{r}) \rangle$  with the order parameter  $\Delta_s(\mathbf{r}_i) = c_{\mathbf{r}_i \uparrow} c_{\mathbf{r}_i \downarrow}$ .

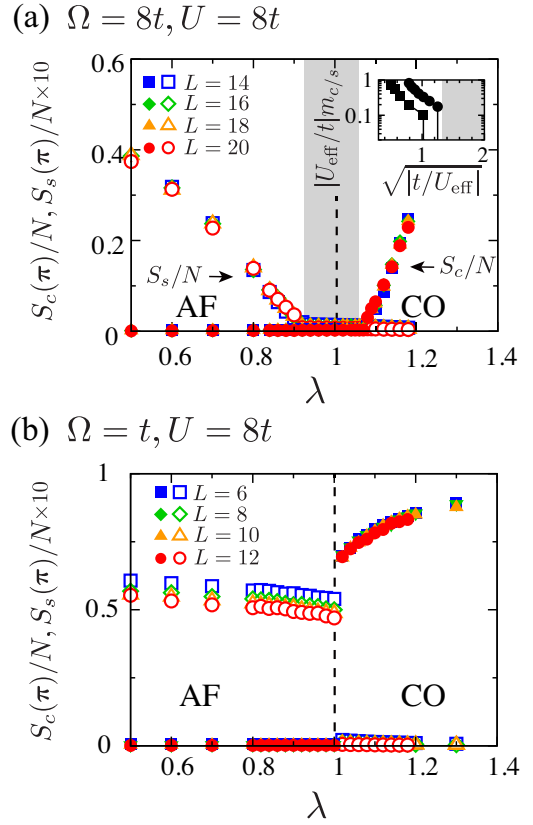


FIG. 2: (Color online) Spin structure factor  $S_s(\pi, \pi)/N$  and charge structure factor  $S_c(\pi, \pi)/N$  as functions of  $\lambda$  at (a)  $(\Omega/t, U/t) = (8, 8)$  and (b)  $(\Omega/t, U/t) = (8, 1)$ , respectively. The vertical dashed line denotes the position where  $U_{\text{eff}} = 0$ . The shaded region indicates the intermediate region where neither the CO nor AF were observed. The inset of (a) shows the plots of  $|U_{\text{eff}}/t|m_c$  (black circles) and  $|U_{\text{eff}}/t|m_s$  (black squares) as a function of  $\sqrt{|t/U_{\text{eff}}|}$ , where  $m_c$  is obtained after the linear extrapolation of  $S_c(\pi, \pi)/N$  as a function of  $1/L$  (See the Supplemental Material).

In Fig. 4, we show physical quantities which were used to determine the phase diagrams. The value of  $S_c(\pi, \pi)/N$  decreases monotonically and the CO eventually disappears at  $\delta \simeq 0.1$  and  $0.22$  for  $\Omega = 8t$  and  $t$ , respectively. On the other hand, the value of  $P_s^\infty$  increases as  $\delta$  increases and we clearly observe a SC state. For small  $\delta$ , a CO and  $s$ -wave SC orders coexist. By the Maxwell construction for the  $\delta - \mu$  curve, however, we find that the SC+CO phase is swallowed up by the PS region in our phase diagrams. Here,  $\mu$  is the chemical potential which was calculated by  $\mu(\bar{N}) = \{E(N_1) - E(N_2)\}/(N_1 - N_2)$ .  $E$  is the total energy and  $\bar{N} = (N_1 + N_2)/2$ . For  $U = 0$ , our Hamiltonian has the particle-hole symmetry at  $\mu = -8\lambda = -2.4$  (for  $\lambda = 0.3$ ). Since this value is above the line used for the Maxwell construction, there is a charge gap at half filling. In our model, the spinodal point  $\delta_s$ , where the uniform charge susceptibility diverges ( $\chi_c^{-1} = \frac{d\mu}{d\rho} = 0$ ), coincides with

the critical point of the CO and therefore the PS is driven by the CO (see also results for the adiabatic limit in the Supplemental Material).

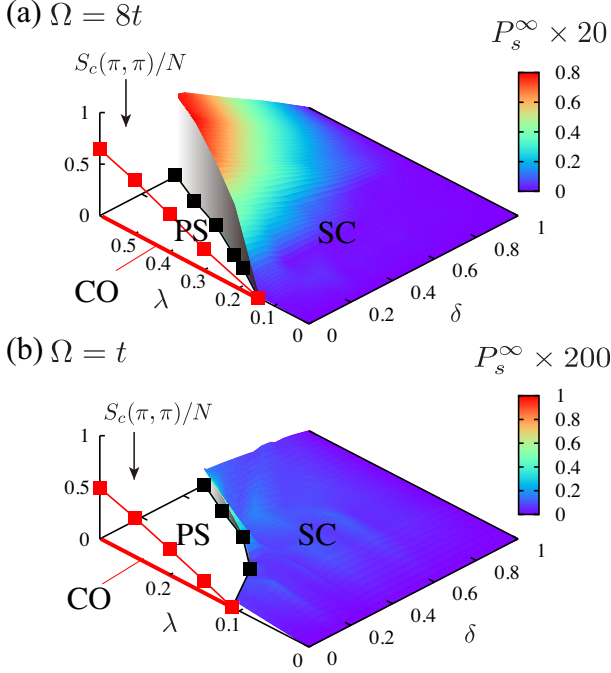


FIG. 3: (Color online) Ground-state phase diagrams of the Holstein model in the  $\delta$ - $\lambda$  plane at (a)  $\Omega = 8t$  and (b)  $\Omega = t$ . In the vertical axis,  $S_c(\pi, \pi)/N$  (red squares) and  $P_s^\infty$  (color plots) for  $L = 14$  are plotted in the CO and SC phase, respectively. Black squares in the bottom plane represent boundaries between phase-separated and  $s$ -wave SC regions. White areas denote the phase-separated regions which were determined from the Maxwell construction. Thick red lines at  $\delta = 0$  indicate the CO phase.

To study the relation between uniform charge fluctuations and superconductivity, we also presented the negative inverse uniform charge susceptibility  $-\chi_c^{-1} = \frac{d\mu}{d\rho}$  in Fig. 4. The PS region associated with the CO is enhanced as  $\Omega$  decreases. In contrast, the SC is suppressed because its main glue for pairing of electrons is the attractive part of the dynamical effective interaction  $U_{\text{eff}}(\omega)$  and the attractive frequency range shrinks for smaller  $\Omega$ . Although SC and PS depend oppositely on  $\Omega$  in this sense, we generally observe the same trend between the enhancement of the  $s$ -wave SC and that of the uniform charge susceptibility for each  $\Omega$ . This feature has been recently observed for  $d$ -wave SC in the Hubbard model[15] and extended  $s$ -wave superconductivity in the *ab-initio* effective Hamiltonian for LaFeAsO[21]. As seen in Fig. 4, the peaks of  $P_s^\infty$  are located at  $\delta \lesssim \delta_s$ , which is reasonable because the effectively strong attraction of carriers induces strongly bound Cooper pairs and it simultaneously leads to the PS. When the system approaches the half filling where it becomes insulating, the SC is suppressed again. The strong attraction is caused

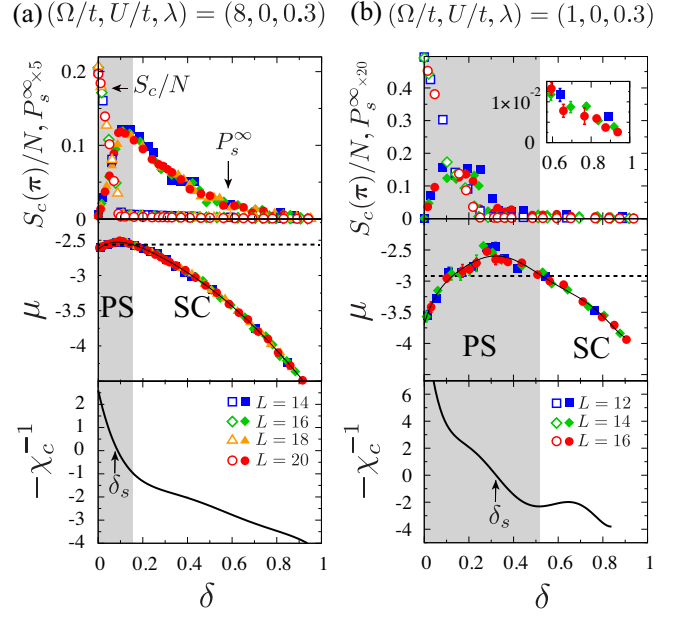


FIG. 4: (Color online) Physical quantities  $S_c(\pi, \pi)/N$ ,  $P_s^\infty$ ,  $\mu$ , and  $-\chi_c^{-1}$  as functions of doping  $\delta$  at (a)  $(\Omega/t, U/t, \lambda) = (8, 0, 0.3)$  and (b)  $(\Omega/t, U/t, \lambda) = (1, 0, 0.3)$ , respectively. The inset of (b) is the enlarge view of  $P_s^\infty$  for large  $\delta$ . The shaded area denotes the phase-separated (PS) region which was determined by the Maxwell construction. The dashed horizontal line in the middle panel is used for the Maxwell construction. The curves of  $-\chi_c^{-1}$  were derived from the derivative of the  $\mu - \delta$  curves (black curves) which were obtained by the 7th order polynomial fit. The spinodal points  $\delta_s$  are indicated as the arrows.

by the electron-phonon interaction while the resultant charge fluctuations may also work as additional glue.

To summarize, by studying the ground-state of the Holstein-Hubbard model on a square lattice, we have clarified where the SC is enhanced if the electron-electron correlation is competing with the coupling to phonons. At half filling, the CO and AF are severely competing, while we have found an intermediate metallic or weakly SC region sandwiched by the CO and AF phases. In the doped case, the SC is dramatically enhanced, but a wide PS region triggered by the CO largely hinders the SC and completely preempts the SC+CO phase. The PS is enhanced for smaller phonon frequencies in contrast to the  $s$ -wave SC. However, we still observe the same trend between the enhancement of the uniform charge susceptibility and those of SC. Then we have revealed that the SC is optimized at the border of the PS. The uniform charge fluctuation may work as an additional glue for phonon-induced on-site  $s$ -wave SC, while main driving force is the attraction mediated by phonons, which drives both PS and SC. These findings have been obtained by the VMC method extended for electron-phonon coupled systems. Our method is quite flexible, and therefore it will



be also useful to study more complicated systems such as *ab initio* Hamiltonians of high  $T_c$  cuprates where several different phonon modes are present.

We thank K. Ido and Y. Murakami for useful discussion. The code was developed based on the open-source software mVMC[39]. This work is financially supported by the MEXT HPCI Strategic Programs for Innovative Research (SPIRE), the Computational Materials Science Initiative (CMSI) and Creation of New Functional Devices and High-Performance Materials to Support Next Generation Industries (CDMSI). This work was also sup-

ported by a Grant-in-Aid for Scientific Research (No. 22104010, No. 22340090 and No. 16H06345) from MEXT, Japan. The simulations were partially performed on the K computer provided by the RIKEN Advanced Institute for Computational Science under the HPCI System Research project (the project number hp130007, hp140215, hp150211, and hp160201). The simulations were also performed on computers at the Supercomputer Center, Institute for Solid State Physics, University of Tokyo.

- 
- [1] A. Y. Ganin, Y. Takabayashi, P. Jeglič, D. Arčon, A. Potočnik, P. J. Baker, Y. Ohishi, M. T. McDonald, M. D. Tzirakis, A. McLennan, et al., *Nature* **1466**, 221 (2010).
  - [2] M. Capone, M. Fabrizio, C. Castellani, and E. Tosatti, *Science* **296**, 2364 (2002).
  - [3] Y. Nomura, S. Sakai, M. Capone, and R. Arita, *Sci. Adv.* **1**, e1500568 (2015).
  - [4] A. Lanzara, P. V. Pogdanov, X. J. Zhou, S. A. Kellar, D. L. Feng, E. D. Lu, T. Yoshida, H. Eisaki, A. Fujimori, K. Kishio, et al., *Nature (London)* **412**, 510 (2001).
  - [5] Z. B. Huang, W. Hanke, E. Arrigoni, and D. J. Scalapino, *Phys. Rev. B* **68**, 220507(R) (2003).
  - [6] S. Ishihara and N. Nagaosa, *Phys. Rev. B* **69**, 144520 (2004).
  - [7] S. Johnston, I. M. Vishik, W. S. Lee, F. Schmitt, S. Uchida, K. Fujita, S. Ishida, N. Nagaosa, Z. X. Shen, and T. P. Devereaux, *Phys. Rev. Lett.* **108**, 166404 (2012).
  - [8] D. Ceperley, G. V. Chester, and M. H. Kalos, *Phys. Rev. B* **16**, 3081 (1977).
  - [9] H. Yokoyama and H. Shiba, *J. Phys. Soc. Jpn.* **80**, 3669 (2011).
  - [10] M. Capello, F. Becca, M. Fabrizio, S. Sorella, and E. Tosatti, *Phys. Rev. Lett.* **94**, 026406 (2005).
  - [11] S. Sorella, *Phys. Rev. B* **64**, 024512 (2001).
  - [12] S. Sorella, *Phys. Rev. B(R)* **71**, 241103 (2005).
  - [13] D. Tahara and M. Imada, *J. Phys. Soc. Jpn.* **77**, 114701 (2008).
  - [14] R. Kaneko, S. Morita, and M. Imada, *J. Phys. Soc. Jpn* **83**, 093707 (2014).
  - [15] T. Misawa and M. Imada, *Phys. Rev. B* **90**, 115137 (2014).
  - [16] S. Morita, R. Kaneko, and M. Imada, *J. Phys. Soc. Jpn* **84**, 024720 (2015).
  - [17] M. Kurita, Y. Yamaji, S. Morita, and M. Imada, *Phys. Rev. B* **92**, 035122 (2015).
  - [18] L. F. Tocchio, F. Becca, A. Parola, and S. Sorella, *Phys. Rev. B* **78**, 041101 (2008).
  - [19] L. F. Tocchio, F. Becca, and C. Gros, *Phys. Rev. B* **83**, 195138 (2011).
  - [20] H. Shinaoka, T. Misawa, K. Nakamura, and M. Imada, *J. Phys. Soc. Jpn* **81**, 034701 (2012).
  - [21] T. Misawa and M. Imada, *Nat. Commun.* **5**, 5738 (2014).
  - [22] M. Hirayama, T. Misawa, T. Miyake, and M. Imada, *J. Phys. Soc. Jpn* **84**, 093703 (2015).
  - [23] T. Ohgoe and M. Imada, *Phys. Rev. B* **89**, 195139 (2014).
  - [24] R. T. Clay and R. P. Hardikar, *Phys. Rev. Lett.* **95**, 096401 (2005).
  - [25] M. Tezuka, R. Arita, and H. Aoki, *Phys. Rev. B* **76**, 155114 (2007).
  - [26] H. Fehske, G. Hager, and E. Jeckelmann, *Europhys. Lett.* **84**, 57001 (2008).
  - [27] J. Bauer, *Phys. Rev. B* **81**, 235113 (2010).
  - [28] Y. Murakami, P. Werner, N. Tsuji, and H. Aoki, *Phys. Rev. B* **88**, 125126 (2013).
  - [29] E. A. Nowadnick, S. Johnston, B. Moritz, R. T. Scalettar, and T. P. Devereaux, *Phys. Rev. Lett.* **109**, 246404 (2012).
  - [30] S. Johnston, E. A. Nowadnick, Y. F. Kung, B. Moritz, R. T. Scalettar, and T. P. Devereaux, *Phys. Rev. B* **87**, 235133 (2013).
  - [31] Y. Murakami, P. Werner, N. Tsuji, and H. Aoki, *Phys. Rev. Lett.* **113**, 266404 (2014).
  - [32] M. Grilli, R. Raimondi, C. Castellani, and C. D. Castro, *Phys. Rev. Lett.* **67**, 259 (1991).
  - [33] R. Raimondi, C. Castellani, M. Grilli, Y. Bang, and G. Kotliar, *Phys. Rev. B* **47**, 3331 (1993).
  - [34] M. C. Gutzwiller, *Phys. Rev. Lett.* **10**, 159 (1963).
  - [35] R. Jastrow, *Phys. Rev.* **98**, 1479 (1995).
  - [36] T. Giamarchi and C. Lhuillier, *Phys. Rev. B* **43**, 12943 (1991).
  - [37] J. E. Hirsch, *Phys. Rev. B* **31**, 4403 (1985).
  - [38] M. Imada, A. Fujimori, and Y. Tokura, *Rev. Mod. Phys.* **70**, 1039 (1998).
  - [39] <https://github.com/issp-center-dev/mVMC>.
  - [40] D. A. Huse, *Phys. Rev. B* **37**, 2380(R) (1998).
  - [41] D. Hurt, E. Odabashian, W. E. Pickett, and R. T. Scalettar, *Phys. Rev. B* **72**, 144513 (2005).
  - [42] C. N. Varney, C.-R. Lee, Z. J. Bai, S. Chiesa, M. Jarrell, and R. T. Scalettar, *Phys. Rev. B* **80**, 075116 (2009).
  - [43] N. Furukawa and M. Imada, *J. Phys. Soc. Jpn.* **61**, 3331 (1992).
  - [44] A. W. Sandvik, *Phys. Rev. B* **56**, 11678 (1997).

# Supplemental Material for “Competitions of Superconducting, Antiferromagnetic and Charge Orders with Intervention by Phase Separation in 2D Holstein-Hubbard Model”

## I. PHASE TRANSITIONS TO AF/CO PHASES AT HALF-FILLING

In the inset of Fig. 2 of the main text, we show the order parameter  $m_{s/c}$  which is defined by  $m_{s/c} = \sqrt{\lim_{L \rightarrow \infty} S_{s/c}(\pi, \pi)/N}$ . In Fig. S1, we show the extrapolation of  $S_{s/c}(\pi, \pi)/N$  to the thermodynamic limit. Here, we plot  $S_{s/c}(\pi, \pi)/N$  as a function  $1/L$  and performed a linear fit based on the spin-wave theory[40]. In order to confirm that the transitions to the AF/CO phases are first-order, we show the existence of energy crossings in Fig. S2.

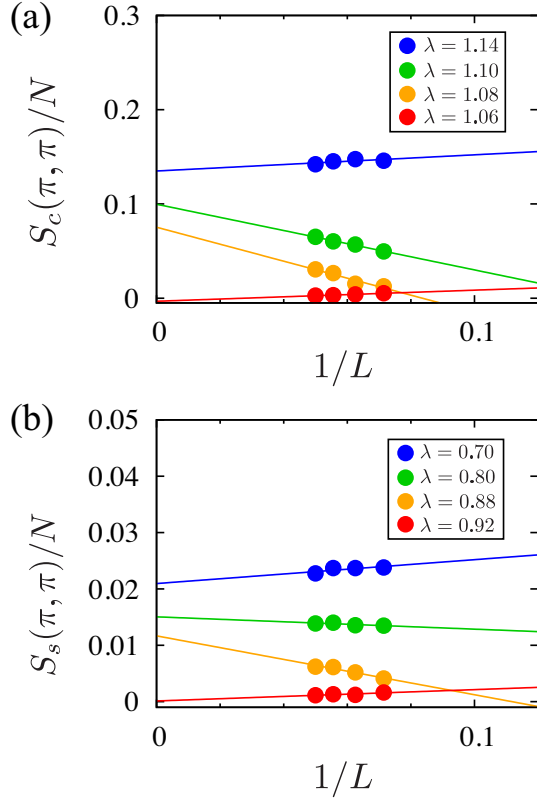


FIG. S1: (Color online) Extrapolations of (a)  $S_s(\pi, \pi)/N$  and (b)  $S_c(\pi, \pi)/N$  to the thermodynamic limit at  $(\rho, \Omega/t, U/t) = (1, 8, 8)$ .

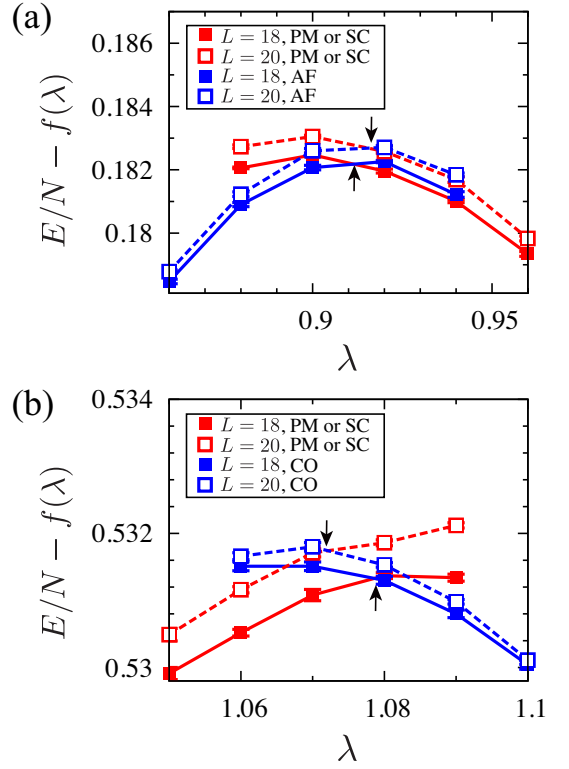


FIG. S2: (Color online)  $E/N - \lambda$  curves of PM or weak SC states and (a) AF/(b) CO states. The linear terms  $f(\lambda) \propto \lambda$  are subtracted for clarity. The crossing points are indicated as arrows.

## II. SUPERCONDUCTING CORRELATION FUNCTION AT HALF FILLING

Here, we show the superconducting correlation functions at half filling and a small effective attraction  $U_{\text{eff}} (< 0)$  where the charge order does not appear. In Fig. S3, we plot the  $s$ -wave superconducting correlation functions  $P_s(\mathbf{r})$  at  $(U/t, \Omega/t, \lambda) = (0, 8, 0.14)$  ( $U_{\text{eff}} = -1.12t$ ).  $P_s(\mathbf{r})$  does not show a clear power-law decay, but instead its long-range parts  $P_s^\infty$  seem to show saturated behaviors. However, after the size extrapolation to the thermodynamic limit[41] (the inset of Fig. S3), its value does not exclude 0 within the error of  $\sim 10^{-4}$ . Because of this extrapolation error, we cannot estimate its value accurately, although it is expected to be finite.

Since our model is mapped onto the attractive Hubbard model with  $U/t = -1.12$  in the antiadiabatic limit  $\Omega/t \rightarrow \infty$  and it is equivalent to the repulsive Hubbard model with  $U/t = 1.12$  at half filling, we may estimate the upper bound of  $P_s^\infty$  from the previous determinant quantum Monte Carlo (DQMC) results of the repulsive Hubbard model[42]. The antiferromagnetic order parameter defined by  $m_s = \sqrt{\lim_{L \rightarrow \infty} S_s(\pi, \pi)/N}$  for the repulsive Hubbard model relates to  $P_s^\infty$  for the attractive Hubbard model as  $P_s^\infty = 2m_s^2$  due to the spin-rotational

symmetry. Since there are no available DQMC data of  $m_s$  for  $U/t < 2$ , we estimate the value at  $U/t = 1.12$  from the rescaled Hartree-Fock result. Here, we rescaled the Hartree-Fock result such that it reproduces the DQMC result at  $U/t = 2$  (shown in Fig. S4), although it seems to overestimate  $m_s$  for  $U/t < 2$ . From this estimation, we obtain  $P_s^\infty \sim 0.001$  for the attractive Hubbard model with  $U/t = -1.12$ . (In the absence of the spin-rotational symmetry which is true for finite  $\Omega/t$ , we need to multiply the additional factor 1.5.) Thus, we confirm that the value of  $P_s^\infty$  for  $\Omega/t = 8$  is smaller than the estimated value for the attractive Hubbard model. We believe that it is mainly due to the retardation effect.

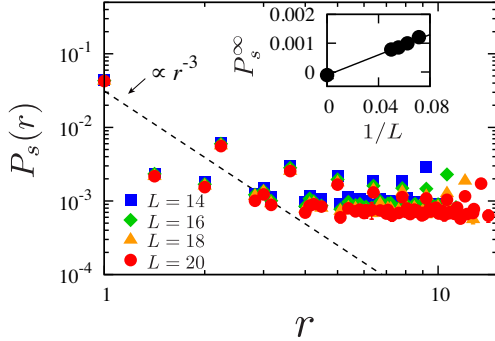


FIG. S3: (Color online) Logarithmic plots of  $P_s(\mathbf{r})$  at  $(\Omega/t, U/t, \lambda) = (8, 0, 0.14)$ . The dashed line represents the asymptotic  $r^{-3}$  scaling for the non-interacting system[43]. In the inset, the extrapolation of  $P_s^\infty$  to the thermodynamic limit is performed by a linear fitting.

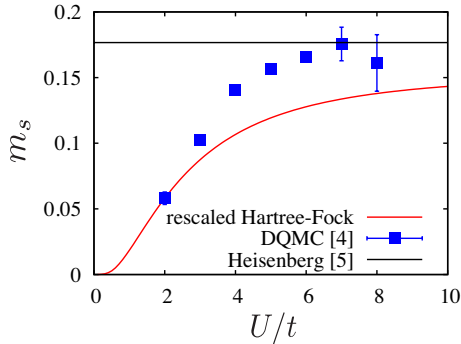


FIG. S4: (Color online) Rescaled Hartree-Fock results of  $m_s$  (red curve). The DQMC results (blue squares) are taken from [42]. Note that our definition of the antiferromagnetic order parameter  $m_s$  is smaller than theirs by factor  $1/(2\sqrt{3})$  due to the difference in the definitions. The result for the Heisenberg model [44] is also shown as the horizontal black line.

### III. PHASE SEPARATION OF THE HOLSTEIN MODEL IN THE ADIABATIC LIMIT

Here, we consider the adiabatic limit  $\Omega/t \rightarrow 0$  of the Holstein model. In this limit, the Hamiltonian reduces to

$$\mathcal{H} = -t \sum_{\langle i,j \rangle, \sigma} (c_{i\sigma}^\dagger c_{j\sigma} + \text{h.c.}) + g \sum_i x_i n_i + \sum_i \frac{K x_i^2}{2}, \quad (2)$$

where  $K$  is the spring constant and the lattice displacements  $\{x_i\}$  become classical variables. By changing variables as  $x_i = \tilde{x}_i - \frac{g}{K}\rho$ , we can rewrite it as

$$\mathcal{H} = -t \sum_{\langle i,j \rangle, \sigma} (c_{i\sigma}^\dagger c_{j\sigma} + \text{h.c.}) + g \sum_i \tilde{x}_i \delta n_i + \sum_i \frac{K \tilde{x}_i^2}{2} - \frac{W\lambda}{2} \rho^2 N. \quad (3)$$

Here,  $\delta n_i = n_i - \rho$  and  $\lambda = \frac{g^2}{KW}$ . In this form, the new lattice displacements  $\{\tilde{x}_i\}$  are 0 if electrons are uniformly distributed ( $\langle \delta n_i \rangle = 0$  for all  $i$ 's).

By completing the square for the second and third terms, the total energy  $\langle \mathcal{H} \rangle$  can be minimized if  $\tilde{x}_i = -\frac{g}{K} \langle \delta n_i \rangle$ . We assume a charge ordered state with  $\tilde{x}_i = (-1)^i x = -\frac{g}{K} \delta n (-1)^i$ , where  $\tilde{x}$  and  $\delta n$  are order parameters. By substituting this for the Hamiltonian, we obtain

$$\mathcal{H} = -t \sum_{\langle i,j \rangle, \sigma} (c_{i\sigma}^\dagger c_{j\sigma} + \text{h.c.}) + g \sum_i \tilde{x} (-1)^i n_i + \frac{K \tilde{x}^2}{2} N - \frac{W\lambda}{2} \rho^2 N. \quad (4)$$

We can diagonalize this by the following unitary transformation:

$$a_{\mathbf{k}\sigma}^\dagger = u_{\mathbf{k}} c_{\mathbf{k}\sigma}^\dagger + v_{\mathbf{k}} c_{\mathbf{k}+\mathbf{Q}\sigma} \quad (5)$$

$$b_{\mathbf{k}\sigma}^\dagger = -v_{\mathbf{k}} c_{\mathbf{k}\sigma}^\dagger + u_{\mathbf{k}} c_{\mathbf{k}+\mathbf{Q}\sigma} \quad (6)$$

with

$$u_{\mathbf{k}}(v_{\mathbf{k}}) = \frac{1}{2} \left[ 1 - (+) \frac{\varepsilon(\mathbf{k})}{\sqrt{\varepsilon(\mathbf{k})^2 + \Delta^2}} \right]. \quad (7)$$

Here,  $\mathbf{Q} = (\pi, \pi)$ . By this transformation, we obtain

$$\mathcal{H} = \sum_{\mathbf{k} \in \text{folded BZ}, \sigma} [E^-(\mathbf{k}) a_{\mathbf{k}\sigma}^\dagger a_{\mathbf{k}\sigma} + E^+(\mathbf{k}) b_{\mathbf{k}\sigma}^\dagger b_{\mathbf{k}\sigma}] + \frac{K \tilde{x}^2}{2} N - \frac{W\lambda}{2} \rho^2 N, \quad (8)$$

with

$$E^\pm(\mathbf{k}) = \pm \sqrt{\varepsilon(\mathbf{k})^2 + \Delta^2} \quad (9)$$

Here, BZ denotes the Brillouin zone,  $\varepsilon(\mathbf{k})$  is the energy dispersion for the non-interacting system and  $\Delta = g\tilde{x}$ . Based on this result, we can numerically calculate the total energy as a function of  $\tilde{x}$  (or  $\delta n$ ) and obtain the ground-state energy as the minimum of  $E(\tilde{x})$ .

In Fig. S5, we present the obtained ground-state phase diagram. In the phase diagram for finite  $\Omega$  (Fig. 3 of the main text), we observe that the phase separation region expands as  $\Omega$  decreases. Especially for large  $\lambda$ , a broad phase separation region is reasonable, because we have the term  $-\frac{W\lambda}{2}\rho^2N$  in the Hamiltonian. The second derivative of  $-\frac{W\lambda}{2}\rho^2$  with respect to  $\rho$  gives the negative constant  $-W\lambda$  and this easily makes the curve of  $E/N$  convex upward for large  $\lambda$ . As is evident, the origin of the term  $-\frac{W\lambda}{2}\rho^2N$  is the uniform shift of the original lattice displacement due to the change of the particle density.

As seen for finite  $\Omega$ , the spinodal point  $\delta_s$  coincides with the critical point of the charge order in the adiabatic limit as well. Actually this is not accidental, because the vanishing  $\Delta$  makes a kink in the chemical potential. To show this, we plot the  $\delta$ -dependence of  $\Delta$  and  $\mu$  in Fig. S6. This fact indicates that the charge order in the doped system is necessarily preempted by the phase separation.

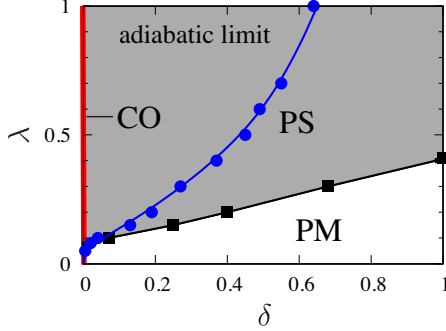


FIG. S5: (Color online) Ground-state phase diagram of the Holstein model (for a  $40 \times 40$  system) in the adiabatic limit. Circles and squares represent the border of the charge order and phase separation, respectively.

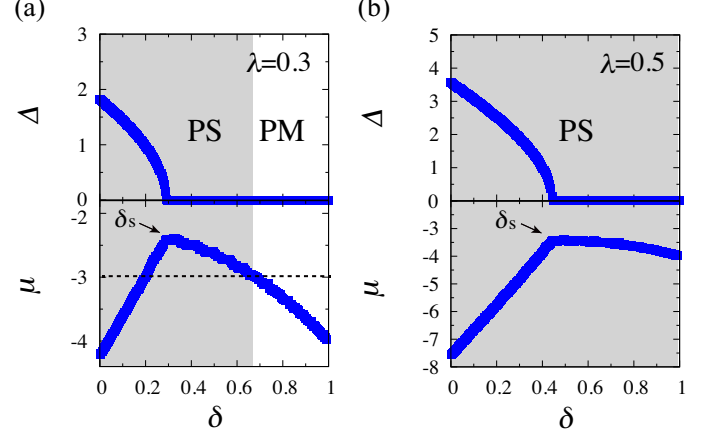


FIG. S6: (Color online)  $\delta$ -dependence of  $\Delta$  and  $\mu$  for (a)  $\lambda = 0.3$  and (b)  $\lambda = 0.5$ . The system size is  $40 \times 40$ . Dashed lines in (a) represent the line for the Maxwell constructions.

- 
- [1] A. Y. Ganin, Y. Takabayashi, P. Jeglič, D. Arčon, A. Potočnik, P. J. Baker, Y. Ohishi, M. T. McDonald, M. D. Tzirakis, A. McLennan, et al., *Nature* **1466**, 221 (2010).
  - [2] M. Capone, M. Fabrizio, C. Castellani, and E. Tosatti, *Science* **296**, 2364 (2002).
  - [3] Y. Nomura, S. Sakai, M. Capone, and R. Arita, *Sci. Adv.* **1**, e1500568 (2015).
  - [4] A. Lanzara, P. V. Pogdanov, X. J. Zhou, S. A. Kellar, D. L. Feng, E. D. Lu, T. Yoshida, H. Eisaki, A. Fujimori, K. Kishio, et al., *Nature (London)* **412**, 510 (2001).
  - [5] Z. B. Huang, W. Hanke, E. Arrigoni, and D. J. Scalapino, *Phys. Rev. B* **68**, 220507(R) (2003).
  - [6] S. Ishihara and N. Nagaosa, *Phys. Rev. B* **69**, 144520 (2004).
  - [7] S. Johnston, I. M. Vishik, W. S. Lee, F. Schmitt, S. Uchida, K. Fujita, S. Ishida, N. Nagaosa, Z. X. Shen, and T. P. Devereaux, *Phys. Rev. Lett.* **108**, 166404 (2012).
  - [8] D. Ceperley, G. V. Chester, and M. H. Kalos, *Phys. Rev. B* **16**, 3081 (1977).
  - [9] H. Yokoyama and H. Shiba, *J. Phys. Soc. Jpn.* **80**, 3669 (2011).
  - [10] M. Capello, F. Becca, M. Fabrizio, S. Sorella, and E. Tosatti, *Phys. Rev. Lett.* **94**, 026406 (2005).
  - [11] S. Sorella, *Phys. Rev. B* **64**, 024512 (2001).
  - [12] S. Sorella, *Phys. Rev. B(R)* **71**, 241103 (2005).
  - [13] D. Tahara and M. Imada, *J. Phys. Soc. Jpn.* **77**, 114701 (2008).



- (2008).
- [14] R. Kaneko, S. Morita, and M. Imada, *J. Phys. Soc. Jpn* **83**, 093707 (2014).
  - [15] T. Misawa and M. Imada, *Phys. Rev. B* **90**, 115137 (2014).
  - [16] S. Morita, R. Kaneko, and M. Imada, *J. Phys. Soc. Jpn* **84**, 024720 (2015).
  - [17] M. Kurita, Y. Yamaji, S. Morita, and M. Imada, *Phys. Rev. B* **92**, 035122 (2015).
  - [18] L. F. Tocchio, F. Becca, A. Parola, and S. Sorella, *Phys. Rev. B* **78**, 041101 (2008).
  - [19] L. F. Tocchio, F. Becca, and C. Gros, *Phys. Rev. B* **83**, 195138 (2011).
  - [20] H. Shinaoka, T. Misawa, K. Nakamura, and M. Imada, *J. Phys. Soc. Jpn* **81**, 034701 (2012).
  - [21] T. Misawa and M. Imada, *Nat. Commun.* **5**, 5738 (2014).
  - [22] M. Hirayama, T. Misawa, T. Miyake, and M. Imada, *J. Phys. Soc. Jpn* **84**, 093703 (2015).
  - [23] T. Ohgoe and M. Imada, *Phys. Rev. B* **89**, 195139 (2014).
  - [24] R. T. Clay and R. P. Hardikar, *Phys. Rev. Lett.* **95**, 096401 (2005).
  - [25] M. Tezuka, R. Arita, and H. Aoki, *Phys. Rev. B* **76**, 155114 (2007).
  - [26] H. Fehske, G. Hager, and E. Jeckelmann, *Europhys. Lett.* **84**, 57001 (2008).
  - [27] J. Bauer, *Phys. Rev. B* **81**, 235113 (2010).
  - [28] Y. Murakami, P. Werner, N. Tsuji, and H. Aoki, *Phys. Rev. B* **88**, 125126 (2013).
  - [29] E. A. Nowadnick, S. Johnston, B. Moritz, R. T. Scalettar, and T. P. Devereaux, *Phys. Rev. Lett.* **109**, 246404 (2012).
  - [30] S. Johnston, E. A. Nowadnick, Y. F. Kung, B. Moritz, R. T. Scalettar, and T. P. Devereaux, *Phys. Rev. B* **87**, 235133 (2013).
  - [31] Y. Murakami, P. Werner, N. Tsuji, and H. Aoki, *Phys. Rev. Lett.* **113**, 266404 (2014).
  - [32] M. Grilli, R. Raimondi, C. Castellani, and C. D. Castro, *Phys. Rev. Lett.* **67**, 259 (1991).
  - [33] R. Raimondi, C. Castellani, M. Grilli, Y. Bang, and G. Kotliar, *Phys. Rev. B* **47**, 3331 (1993).
  - [34] M. C. Gutzwiller, *Phys. Rev. Lett.* **10**, 159 (1963).
  - [35] R. Jastrow, *Phys. Rev.* **98**, 1479 (1995).
  - [36] T. Giamarchi and C. Lhuillier, *Phys. Rev. B* **43**, 12943 (1991).
  - [37] J. E. Hirsch, *Phys. Rev. B* **31**, 4403 (1985).
  - [38] M. Imada, A. Fujimori, and Y. Tokura, *Rev. Mod. Phys.* **70**, 1039 (1998).
  - [39] <https://github.com/issp-center-dev/mVMC>.
  - [40] D. A. Huse, *Phys. Rev. B* **37**, 2380(R) (1998).
  - [41] D. Hurt, E. Odabashian, W. E. Pickett, and R. T. Scalettar, *Phys. Rev. B* **72**, 144513 (2005).
  - [42] C. N. Varney, C.-R. Lee, Z. J. Bai, S. Chiesa, M. Jarrell, and R. T. Scalettar, *Phys. Rev. B* **80**, 075116 (2009).
  - [43] N. Furukawa and M. Imada, *J. Phys. Soc. Jpn.* **61**, 3331 (1992).
  - [44] A. W. Sandvik, *Phys. Rev. B* **56**, 11678 (1997).